A&A 478, 71–81 (2008)
DOI: 10.1051/0004-6361:20077118


Astronomy & Astrophysics

# Geometrical tests of cosmological models

## III. The Cosmology-evolution diagram at $z = 1$

C. Marinoni[1], A. Saintonge[2], T. Contini[3], C. J. Walcher[4], R. Giovanelli[2], M. P. Haynes[2], K. L. Masters[5], O. Ilbert[4], A. Iovino[6], V. Le Brun[4], O. Le Fevre[4], A. Mazure[4], L. Tresse[4], J.-M. Virey[1], S. Bardelli[7], D. Bottini[8], B. Garilli[8], G. Guzzo[9], D. Maccagni[8], J. P. Picat[3], R. Scaramella[9], M. Scodeggio[8], P. Taxil[1], G. Vettolani[10], A. Zanichelli[10], and E. Zucca[7]

[1] Centre de Physique Théorique*, CNRS-Université de Provence, Case 907, 13288 Marseille, France
e-mail: marinoni@cpt.univ-mrs.fr
[2] Department of Astronomy, Cornell University, Ithaca, NY 14853, USA
[3] Laboratoire d'Astrophysique de l'Observatoire Midi-Pyrénées, UMR 5572, 31400 Toulouse, France
[4] Laboratoire d'Astrophysique de Marseille, UMR 6110, CNRS Université de Provence, 13376 Marseille, France
[5] Harvard-Smithsonian Center for Astrophysics, Cambridge, MA 02143, USA
[6] INAF-Osservatorio Astronomico di Brera, via Brera 28, 20121 Milano, Italy
[7] INAF-Osservatorio Astronomico di Bologna, via Ranzani 1, Bologna, Italy
[8] IASF-INAF, via Bassini 15, 20133 Milano, Italy
[9] INAF-Osservatorio Astronomico di Brera, via Bianchi 46, 23807 Merate, Italy
[10] IRA-INAF, via Gobetti, 101, 40129 Bologna, Italy

Received 17 January 2007 / Accepted 6 September 2007

**ABSTRACT**

The rotational velocity of distant galaxies, when interpreted as a size (luminosity) indicator, may be used as a tool to select high redshift standard rods (candles) and probe world models and galaxy evolution via the classical angular diameter-redshift or Hubble diagram tests. We implement the proposed testing strategy using a sample of 30 rotators spanning the redshift range $0.2 < z < 1$ with high resolution spectra and images obtained by the VIMOS/VLT Deep Redshift Survey (VVDS) and the Great Observatories Origins Deep Survey (GOODs). We show that by applying at the same time the angular diameter-redshift and Hubble diagrams to the same sample of objects (i.e. velocity selected galactic discs) one can derive a characteristic chart, the cosmology-evolution diagram, mapping the relation between global cosmological parameters and local structural parameters of discs such as size and luminosity. This chart allows to put constraints on cosmological parameters when general prior information about discs evolution is available. In particular, by assuming that equally rotating large discs cannot be less luminous at $z = 1$ than at present ($M(z = 1) \lesssim M(0)$), we find that a flat matter dominated cosmology ($\Omega_{\rm m} = 1$) is excluded at a confidence level of $2\sigma$ and an open cosmology with low mass density ($\Omega_{\rm m} \sim 0.3$) and no dark energy contribution ($\Omega_\Lambda$) is excluded at a confidence level greater than $1\sigma$. Inversely, by assuming prior knowledge about the cosmological model, the cosmology-evolution diagram can be used to gain useful insights about the redshift evolution of baryonic discs hosted in dark matter halos of nearly *equal masses*. In particular, in a $\Lambda CDM$ cosmology, we find evidence for a bimodal evolution where the low-mass discs have undergone significant surface brightness evolution over the last 8.5 Gyr, while more massive systems have not. We suggest that this dichotomy can be explained by the epochs at which these two different populations last assembled.

**Key words.** cosmology: observations – cosmology: cosmological parameters – galaxies: fundamental parameters – galaxies: evolution –
galaxies: high-redshift

## 1. Introduction

Deep redshift surveys of the Universe, such as the VIMOS/VLT deep redshift survey (VVDS, Le Fèvre et al. 2005) and the ACS/zCOSMOS survey (Lilly et al. 2006) are currently underway to study the physical properties of high redshift galaxies. Motivated by these major observational efforts, we are currently exploring whether high redshift galaxies can also be used as cosmological tracers. Specifically, we are trying to figure out if these new and large sets of spectroscopic data can be meaningfully used to probe, in a geometric way, the value of the constitutive parameters of the Friedmann-Robertson-Walker cosmological model.

A whole arsenal of classical geometrical methods has been developed to measure global properties of the universe. The central feature of all these tests is the attempt to probe the various operative definitions of relativistic distances by means of scaling relationships in which a distant dependent observable, (e.g. an angle or a flux), is expressed as a function of a distance independent fixed quantity (e.g. metric size or absolute luminosity).

A common thread of weakness in all these approaches to measure cosmological parameters using distant galaxies or

* Centre de Physique Théorique is UMR 6207 – "Unité Mixte de Recherche" of CNRS and of the Universities "de Provence", "de la Méditerranée" and "du Sud Toulon-Var" – Laboratory affiliated to FRUMAM (FR 2291).

AGNs selected in deep redshift surveys is that there are no clear criteria by which such cosmological objects should be considered universal standard rods or standard candles.

Motivated by this, in previous papers (Marinoni et al. 2004; Marinoni et al. 2008, hereafter Paper I) we have investigated the possibility of using the observationally measured and theoretically justified correlation between size/luminosity and disc rotation velocity as a viable method to select a set of high redshift galaxies, with statistically homologous dimensions/luminosities. This set of tracers may be used to test the evolution of the cosmological metric via the implementation of the standard angular diameter-redshift and Hubble diagram tests.

Finding valid standard rods, however, does not solve the whole problem; the implementation of the angular diameter-redshift test using distant galaxies is hampered by the difficulty of disentangling the effects of galaxy evolution from the signature of geometric expansion of the universe.

In Paper I we have determined some general conditions under which galaxy kinematics may be used to test the evolution of the cosmological metric. We have shown that in the particular case in which disc evolution is linear and modest (<30% at $z = 1.5$), the inferred values of the dark energy density parameter $\Omega_Q$ and of the cosmic equation of state parameter $w$ are minimally biased ($\delta\Omega_Q = \pm 0.15$ for any $\Omega_Q$ in the range $0 < \Omega_Q < 1$).

In Paper I, we also looked for cosmological predictions that rely on less stringent assumptions, i.e. which do not require specific knowledge about the particular functional form of the standard rod/candle evolution. In particular, we showed how velocity-selected rotators may be used to construct a *cosmology-evolution diagram* for disc galaxies. This is a chart mapping the local physical parameter space of rotators (absolute luminosity and disc linear size) onto the space of global, cosmological parameters ($\Omega_{\rm m}$, $\Omega_Q$). Using this diagram it is possible to extract information about cosmological parameters once the amount of size/luminosity evolution at some reference epoch is known. Vice-versa, once a cosmological model is assumed, the cosmology-evolution mapping may be used to directly infer the specific time evolution in magnitude and size of disc galaxies that are hosted *in dark matter halos of similar mass*.

We stress that this last way of reading the cosmology-evolution diagram offers a way to explore galaxy evolution which is orthogonal to more traditional methods. In particular, insights into the mechanisms of galaxy evolution are traditionally accessible through the study of disc galaxy scaling relations, such as the investigation of the time-dependent change in the magnitude-velocity (Tully-Fisher) relation (e.g., Vogt et al. 1996; Böhm et al. 2004; Bamford et al. 2006), of the magnitude-size relations (e.g., Lilly et al. 1998; Simard et al. 1999; Bouwens & Silk 2002; Barden et al. 2005), or of the disc "thickness" (Reshetnikov et al. 2003; Elmegreen et al. 2005). By applying the angular size-redshift test and the Hubble diagram to velocity-selected rotators, we aim at tracing the evolution in linear size, absolute magnitude and intrinsic surface brightness of disc galaxies that are hosted halos of the same given mass at every cosmic epoch explored.

In this paper, we present a pilot observational program that allowed us to test whether galaxy rotational velocity can be used to select standard rods, and to derive the cosmology-evolution diagram for disc galaxies at redshift $z = 1$. Our observing strategy was to follow-up in medium resolution spectroscopic mode with VIMOS a set of emission-line objects selected from a sample of galaxies in the Chandra Deep Field South (CDFS) region for which high resolution photometric parameters were available (Giavalisco et al. 2004).

The outline of the paper is as follow: in Sect. 2 we describe the VVDS spectroscopic data taken in the CDFS region. In Sect. 3 we outline a strategy to test the consistency of the standard rod/candle selection. In Sect. 4 we derive the cosmology-evolution diagram for our sample of rotators, and in Sect. 5 we present our results about disc size, luminosity and surface brightness evolutions. Discussions and conclusions are presented in Sects. 6 and 7, respectively. Throughout, the Hubble constant is parameterized via $h_{70} = H_0/(70\ {\rm km\,s^{-1}\,Mpc^{-1}})$. All magnitudes in this paper are in the AB system (Oke & Gunn 1983), and from now the AB suffix will be omitted.

## 2. Sample: observations and data reduction

Our strategy to obtain kinematic information for the largest possible sample of rotators at high redshift was to re-target in medium resolution mode ($R = 2500$) galaxies in the CDFS region for which a previous pass in low-resolution mode (Le Fèvre et al. 2004) already provided spectral information such as redshifts, emission-line types, and equivalent widths, for galaxies down to $I = 24$. Galaxies were selected as rotators if their spectra was blue and characterized by emission line features (OII, H$\beta$, OIII, H$\alpha$). CDFS photometry was then used to confirm the disc-like nature of their light distribution (i.e. the absence of any strong bulge component), and also to avoid including in the sample objects with peculiar morphology or undergoing merging or interaction events.

The final sample of candidates for medium resolution retargeting was defined by further requiring that the inclination of the galaxy be greater than 60° to minimize biases in velocity estimation, and that its identified emission line fall on the CCD under the tighter constraints imposed by the medium resolution grism. Once the telescope pointing and slit positioning were optimized using the low-resolution spectral information, the remaining space on the focal plane mask was blindly assigned to galaxies in the field.

Spectroscopic observations have been obtained with the VIMOS spectrograph on the VLT Melipal telescope in October 2002. The slit width was 1 arcsec giving a spectral resolution $R = 2500$ as measured on the FWHM of arc lines. Using the VIMOS mask design software and capabilities of the slit-cutting laser machine (Bottini et al. 2005), slits have been placed on each galaxy at a position angle aligned with the major axis. The seeing at the time of observations was 0.8 arcsec FWHM with an integration time of 1h30 split in three exposures of 30 min each.

Most of the galaxies in the CDFS area surveyed by the VVDS have high resolution images taken with the ACS camera of the HST by GOODs. Images are available in four different filters (*F435W*, *F606W*, *F775W*, *F850LP*) noted hereafter *B*, *V*, *I* and *Z*, respectively. A small fraction of the targeted galaxies has only *I* band images provided by the ESO Imaging Survey (Arnouts et al. 2001).

The galaxy rotational velocity has been estimated using the linewidths of the emission lines. A detailed analysis of the velocity extraction algorithm and of the potential systematic errors implicit in this technique are presented in Paper II of this serie (Saintonge et al. 2008). This technique to measure rotation velocities imposed itself since many galaxies at high redshift were too small to measure rotation curves reliably, and since summing all the light to form velocity histograms increased the signal-to-noise ratio (S/N) of the detected lines.

Magnitudes have been computed in the $I$ band and a K-correction was applied (see Ilbert et al. 2005 for a detailed discussion). They were also corrected for galactic absorption using the maps of Schlegel et al. (1998) in the CDFS region (i.e. on average a correction of ∼0.0016), and for galaxy inclination by adopting a standard empirical description of internal extinction $A_\lambda$ in the pass-band $\lambda$, $\gamma \log(\sec i)$, where $i$ is the galaxy inclination angle as calculated from the galaxy axis ratio and $\gamma_I = 0.92 + 1.63(\log 2v - 2.5)$ (Tully et al. 1998) where $v$ is the maximum rotational velocity of a galaxy.

Galaxy sizes have been specified in terms of the half-light diameter (HLD) inferred in the $I$ band. Typical errors in the measurements are $\sigma_\theta \sim 0.04''$. In Paper I we stressed the importance of using a metric rather than an isophotal definition of galaxy diameters for cosmological purposes (e.g. Sandage 1995). We also verified that the HLDs for our sample of galaxies do not depend on wavelength; there is no systematic difference in the inferred metric diameters when the HLD is computed in the $B$, $V$, $I$ or $z$ filters (see also Sandage & Perelmuter 1990; de Jong 1996). The scatter in the HLDs inferred in different bands is of order $0.02''$ and therefore small in comparison to the observational uncertainties $\sigma_\theta$.

[OII] linewidths have been translated into an estimate of the galaxy rotational velocity, $v$, as detailed in Sect. 3.2 of Paper II. Rotational velocity was derived using [OII](3727 Å) lines (24 objects), [OIII](5007 Å) lines (10 objects) and H$\alpha$(6563 Å) (5 objects). 23 galaxies have velocities in the range $0 < v(\mathrm{km\ s^{-1}}) \leq 100$ (with mean velocity of the sample ∼60 km s$^{-1}$) and 16 galaxies have velocities in the range $100 < v(\mathrm{km\ s^{-1}}) \leq 200$ (with mean velocity of the sample ∼143 km s$^{-1}$) .

After data reduction, we were left with a sample of 39 objects, 27 of which have high resolution imaging. As for the remaining objects with ground photometry, we only consider in the following those with $z < 0.2$, in order to exclude faint and small galaxies for which the size measurements are severely compromised by seeing distortions. Therefore, our final "science" sample contains 30 objects.

Data are organized and presented in Table 1 as follows: Col. 1: galaxy ID in the EIS catalog, Col. 2: redshift, Col. 3, rotation velocity, Col. 4: half-light angular radius, Col. 5: magnitude, Col. 6: surface brightness within the half-light radius.

**Table 1.** Properties of the galaxy sample.

| EIS ID | $z$ | $v$(km s$^{-1}$) | $\theta^o$(arcsec) | $m^o$ | $\mu^o$ (mag/arcsec$^2$) |
|---|---|---|---|---|---|
| 30445 | 0.9332 | 97 | 0.180 | 23.744 | 22.03 |
| 32177 | 0.8934 | 68 | 0.149 | 23.681 | 21.54 |
| 31328 | 0.4164 | 79 | 0.606 | 22.297 | 23.20 |
| 32998 | 0.1464 | 28 | 0.857 | 20.794 | 22.45 |
| 34826 | 0.4559 | 204 | 0.715 | 22.684 | 23.95 |
| 34244 | 0.5321 | 55 | 0.298 | 22.324 | 21.69 |
| 29895 | 0.6807 | 44 | 0.220 | 23.571 | 22.23 |
| 37157 | 0.8677 | 129 | 0.751 | 23.399 | 24.77 |
| 33200 | 0.1267 | 96 | 0.806 | 20.519 | 22.04 |
| 33763 | 1.0220 | 130 | 0.755 | 23.404 | 24.79 |
| 31501 | 1.0360 | 140 | 0.747 | 23.513 | 24.87 |
| 31194 | 0.3320 | 80 | 0.818 | 21.950 | 23.51 |
| 29342 | 0.4680 | 55 | 0.481 | 23.565 | 23.97 |
| 29232 | 0.8610 | 155 | 0.370 | 22.320 | 22.15 |
| 34325 | 0.3334 | 26 | 0.221 | 23.570 | 22.20 |
| 34560 | 0.8618 | 28 | 0.204 | 23.549 | 22.00 |
| 36484 | 0.7539 | 25 | 0.202 | 23.781 | 22.30 |
| 16401 | 1.1000 | 306 | 0.913 | 21.628 | 23.42 |
| 17811 | 0.8143 | 170 | 0.726 | 23.573 | 24.87 |
| 17362 | 0.6814 | 178 | 0.683 | 22.379 | 23.54 |
| 22685 | 0.8411 | 115 | 0.891 | 22.147 | 23.88 |
| 17255 | 0.1787 | 99 | 1.203 | 21.758 | 24.16 |
| 15152 | 0.7931 | 169 | 0.895 | 21.702 | 23.46 |
| 15099 | 0.3661 | 70 | 0.509 | 21.171 | 21.70 |
| 19702 | 0.6770 | 62 | 0.295 | 22.812 | 22.16 |
| 16377 | 0.5621 | 36 | 0.490 | 22.944 | 23.37 |
| 17421 | 0.7834 | 99 | 0.361 | 23.280 | 23.06 |
| 20202 | 0.5763 | 26 | 0.190 | 23.318 | 21.70 |
| 18416 | 0.8859 | 99 | 0.205 | 23.637 | 22.18 |
| 17534 | 0.3493 | 35 | 0.271 | 23.837 | 22.99 |
| 15486 | 0.6613 | 146 | 0.551 | 22.495 | 23.20 |
| 19684 | 0.8588 | 104 | 0.424 | 22.790 | 22.92 |
| 18743 | 0.6800 | 81 | 0.447 | 22.950 | 22.70 |
| 15553 | 0.4584 | 183 | 0.991 | 19.292 | 21.26 |
| 18417 | 0.5350 | 36 | 0.342 | 22.877 | 22.54 |
| 18779 | 0.5623 | 59 | 0.351 | 22.445 | 22.15 |
| 21252 | 0.5795 | 102 | 0.414 | 22.854 | 22.93 |
| 20708 | 0.1228 | 166 | 1.540 | 18.427 | 21.40 |
| 18853 | 0.6509 | 116 | 0.556 | 21.350 | 22.10 |

## 3. Selection of standard rods/candles

An observable relationship exists between the metric radial dimension $D$ of a disc and its speed of rotation $v$. An analogous empirical relationship connects rotation with luminosity (Tully & Fisher 1977). In Paper I we have proposed to use information on the kinematics of galaxies, as encoded in their OII emission-line width, to *objectively* identify standard rods/candles at high redshifts. A discussion of the requirements and of the optimal strategies to fulfill this observational program is detailed in Paper I.

A variety of standard rod candidates have been explored in previous attempts of providing a direct geometrical proof of the curvature of the universe. A common thread of weakness in all these attempts is that there are no clear physical nor statistical criteria by which the proposed objects (clusters, extended radio lobes or compact radio jets associated with quasars and AGNs) should be considered universal standard rods/candle.

Even assuming that a particular class of standards is identified, the length of the rod remains unknown. Since the inferred cosmological parameters heavily depend on the assumed value for the object size (Lima & Alcaniz 2000), an a-priori independent statistical study of the standard rod absolute calibration is an imperative prerequisite. In Paper II, we used a large sample of galaxies from the SFI++ catalog (Springob et al. 2007) to fix the local calibration values for absolute magnitudes and linear diameters of galaxies with a given rotational velocity.

### 3.1. Velocity selection of rotators: test of consistency

We have seen that, in order to implement the proposed test, we need two sample of rotators: the "data sample" (galaxies with the same rotational velocity selected over the widest possible redshift range; the sample presented in Sect. 2), and the "calibration sample" (rotators at redshift $z \sim 0$ for which the physical size of the linear diameter is known; the SFI++ sample analyzed in Paper II). This last sample allows us to calibrate the zero-point of the Hubble and angular size-redshit diagrams (i.e. $M_v(0)$ and $D_v(0)$ in Eqs. (2) an (4)).

We stress that the disc rotational velocity of galaxies in the two samples is measured using two different velocity indicators (spectroscopic lines) and two different velocity extraction methods. Specifically we use OII linewidths to measure the rotational velocity of the distant "data" sample and $H_\alpha$

rotation curves to measure the velocities of the local "calibration" galaxies. Therefore, it is imperative to check that possible biases or errors introduced by combining velocities inferred using systematically different measuring techniques do not prevent a meaningful comparison between different samples at different redshifts.

To this purpose we have implemented the following testing strategy. Given a spectroscopically-selected sample of standard candles $M_v(0)$ with rotational velocity $v$, one can derive the observed apparent magnitude $m^{\rm o}$ of a standard candle located at redshift $z$, by using the relation (Sandage 1988):

$$m^{\rm o} = m^{\rm th}(M_v(0), z, \boldsymbol{p}) + \epsilon_{\rm M}(z, \boldsymbol{p}) + K(z) \quad (1)$$

where

$$m^{\rm th} = M_v(0) + 5\log d_{\rm L}(z, \boldsymbol{p}) + 25 \quad (2)$$

and where $d_{\rm L}(z, \boldsymbol{p})$ is the luminosity distance (depending on the set of cosmological parameters $\boldsymbol{p}$), $K(z)$ is the K-correction term and $\epsilon_{\rm M}(z, \boldsymbol{p})$ is the a priori unknown cosmology-dependent evolution in luminosity of our standard candle, i.e. $\epsilon_{\rm M}(z, \boldsymbol{p}) = M_v(z, \boldsymbol{p}) - M_v(0)$ is the difference between the absolute magnitude of an object of rotational velocity $v$ measured at redshift $z$ with respect to the un-evolved local standard value $M_v(0)$.

Similarly, one can parameterize any possible evolution affecting the standard rod $D_v(0)$ by writing its observed apparent subtended angle at redshift $z$ as

$$\theta^0 = \theta^{\rm th}(D_v(0), z, \boldsymbol{p})[1 + \delta(z, \boldsymbol{p})] \quad (3)$$

where the theoretically expected angular scaling ($\theta^{\rm th}$) is given by

$$\theta^{\rm th} = \frac{D_v(0)}{d_{\rm A}(z, \boldsymbol{p})}, \qquad d_{\rm A} = d_{\rm L}(1+z)^{-2} \quad (4)$$

and where $\delta(z, \boldsymbol{p})$ is a cosmology-dependent function which describes the relative redshift evolution of the standard rod, i.e. $\delta \equiv (D_v(z, \boldsymbol{p}) - D_v(0))/D_v(0) \equiv \epsilon_D/D_v(0)$. We note that any possible evolution in the standard rod angular size is related to the evolution in its linear dimension as follows: $\epsilon_\theta = \epsilon_D/d_{\rm A}$. Here and in the following, we assume that the angular size of fixed-velocity rotators is estimated using the galaxy half-light diameter $D_v$.

From the definition of wavelength-specific surface brightness, $\mu$, we deduce that the variation as a function of redshift in the average intrinsic surface brightness within a radius $R$ for our set of velocity selected galaxies (i.e. $\Delta\langle\mu^{\rm in}(z)\rangle_R \equiv \langle\mu^{\rm in}(z) - \mu^{\rm in}(0)\rangle_R$) is

$$\Delta\langle\mu^{\rm in}(z)\rangle_R = \Delta M_v(<R) + 5\log\frac{R(z)}{R(0)}. \quad (5)$$

By choosing the half-light diameter $D_v$ as a metric definition for the size of a standard rod, we immediately obtain the intrinsic surface brightness evolution within $D_v$ as

$$\Delta\langle\mu^{\rm in}(z)\rangle_{D_v} = \epsilon_{\rm M}(z, \boldsymbol{p}) + 5\log(1 + \delta(z, \boldsymbol{p})). \quad (6)$$

While the specific amount of evolution in luminosity and size do in principle depend on the specific background cosmological model adopted, the corresponding evolution in intrinsic surface brightness is a cosmology-independent quantity.

The evolution in intrinsic surface brightness is not a directly measurable quantity, but, in a FRW metric, this quantity can be easily related to the apparent surface brightness change observed in a waveband $\Delta\lambda$ by the relation

$$\Delta\langle\mu^{\rm o}(z)\rangle_{D_v} = \Delta\langle\mu^{\rm in}(z)\rangle_{D_v} + 2.5\log(1+z)^4 + K(z). \quad (7)$$

**Table 2.** Local calibration for diameters, absolute magnitudes and surface brightness within the half light radius as derived in Paper II.

| $\langle v\rangle$/(km s$^{-1}$) | $D(0)/(h_{70}^{-1}$ kpc) | $M(0) - 5\log h_{70}$ | $\mu(0)$ (mag/arcsec$^2$) |
|---|---|---|---|
| 60 | $4.30 \pm 2.8$ | $-18.80 \pm 0.75$ | $21.50 \pm 0.74$ |
| 143 | $9.00 \pm 2.5$ | $-21.40 \pm 0.44$ | $20.45 \pm 0.70$ |

We note that the left-hand side of Eq. (7) is directly measurable using photometric images. Moreover, it can be measured without assuming any specific galaxy light profile and it will be, in general, a non linear function of redshift. By combining Eqs. (1), (3), (6) and (7) we define the $\eta$ function:

$$\eta = m^{\rm o}(z) - \Delta\langle\mu^{\rm o}(z)\rangle_{D_v} + 5\log\theta^{\rm o}(z). \quad (8)$$

The specific combination in Eq. (8) of observed magnitudes, half-light diameters, and evolution in the observed surface brightness within the HLD ($\Delta\langle\mu^{\rm o}(z)\rangle_{D_v} = \langle\mu^{\rm o}(z)\rangle_{D_v} - \langle\mu^{\rm o}(0)\rangle_{D_v}$) is, by construction, a redshift-invariant quantity which is equal to

$$\eta = M_v(0) + 5\log D_v(0) + 25. \quad (9)$$

From a theoretical point of view, we emphasize that the $\eta$-estimator given in Eq. (8) does not explicitly depend on i) K correction, ii) evolution in luminosity or size of our standard sources and iii) on the specific gravitational model assumed to derive the exact functional form of the angular and luminosity distances.

From an observational point of view, we stress that Eq. (8) can be directly estimated using photometric images of the "data" sample, while Eq. (9) may be expressed in terms of the locally measured absolute magnitudes and linear diameters of our "calibration" sample. Therefore, by simply comparing the values of the $\eta$ function inferred using the "data" sample (Eq. (8)) with the constant value predicted using the "calibration" sample (Eq. (9)), we can test for the presence of eventual biases in our data. The goal is to reveal possible systematics that could be introduced, for example, by the different techniques with which rotation properties are inferred locally (mainly using $H_\alpha$ rotation curves) and at higher redshift (mainly using OII line-widths). Clearly, a mismatch would indicate that our spectroscopic selection technique fails in selecting homologous classes of objects embedded in halos of nearly the same mass at different redshifts.

Since our total sample is still limited, at present it is practical to implement the proposed test of consistency by defining only two broad classes of velocity-selected galaxies: a low-velocity sample of standard rods/candles with $0 < v \leq 100$ km s$^{-1}$ containing 22 galaxies with mean rotational velocity of $\sim$60 km s$^{-1}$ ($S_{60}$ sample) and a high-velocity set of objects with $100 < v < 200$ km s$^{-1}$ containing 8 rotators with mean velocity of $\sim$143 km s$^{-1}$ ($S_{143}$ sample). The size (HLD), absolute luminosity and mean surface brightness $\mu(0)$ within the HLD of local galaxies are derived using the calibration relationships of Paper II and are quoted in Table 2. Clearly, with more high resolution data becoming available, it will be possible to split the sample in finer velocity bins and thus select standard rods/candles having smaller size/luminosity dispersions.

In Fig. 1 we plot the $\eta$-estimator (see Eq. (8)) for the $S_{60}$ sample of rotators. The first and third terms on the RHS of Eq. (8) were estimated as explained in Sect. 2, while the second term was evaluated by fitting the observed SB with a linear model and subtracting from the observation the zero point of the model (i.e. the value $\langle\mu^0(0)\rangle$ inferred using the linear model).

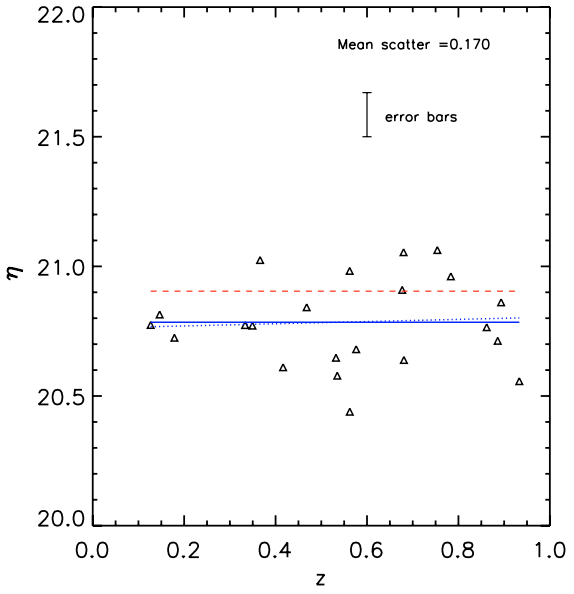


**Fig. 1.** The $\eta$ estimator scatter plot computed using Eq. (8) and the $S_{60}$ sample. The dotted line is the best fitted linear regression to the data, while the solid line represents the best fitted constant model. The dashed line represents the estimated values for the $\eta$ function obtained by using locally calibrated values for the standard rods and candles, i.e. using Eq. (9) with the values specified in Table 2. The best fitting linear regression is consistent with being a constant function of redshift.

A series of conclusions can be immediately drawn. First, the best fitting linear regression is very well approximated by a constant function of redshift. This *shape* is not only theoretically expected, but it is consistent with the hypothesis that none of the relevant photometric parameters (angular sizes, magnitudes, surface brightnesses) measured for our sample of rotators suffer from any redshift-dependent systematics.

Secondly, the consistency of the measurements can be assessed by comparing the *scatters* in $\eta$ estimated by using Eqs. (8) and (9). The average scatter in Eq. (8) measures the quality with which angular diameters, magnitudes and surface brightnesses have been measured in the "data" sample. This is an extremely useful indicator since measuring structural parameters for distant, faint and small galaxies is not an error-free task. $\sigma_\eta$ is thus a quality parameter which describes the overall consistency of our measurements of the three observables $m^{\rm o}, \mu^{\rm o}$ and $D^{\rm o}$. The average scatter in Eq. (9) indicates the robustness with which local velocity data can be used to select standard candles/rods. In other terms it reflects the intrinsic scatter in the calibration of the Tully-Fisher relation for local diameters and magnitudes. Clearly, if scatter in Eq. (8) is comparable or bigger than scatter in Eq. (9), then our high redshift data would be of low quality and definitely useless. The scatter in Eq. (8) ($\sigma_\eta = 0.035$) is nearly one order of magnitude smaller than that inferred using Eq. (9) (∼0.3), and, together with the absence of any trend in the distribution of the residuals, shows that the photometric parameters of the "data" sample have been consistently determined over all the redshift baseline.

Finally, the *normalization* of this constant function tells us about the effectiveness of our kinematic measurements (i.e. about the homogeneity of the sample of velocity-selected rotators). The fact that the $\eta$-value inferred using the "data" sample of rotators with $v = 60$ km s$^{-1}$ (Eq. (8)) is well within the errors of the $\eta$ value estimated using Eq. (9) and our local "calibration" sample (∼0.3) allows us to conclude that both the high redshift sample and the local one are homogeneously selected in velocity space. The low redshift counterparts of our rotators have a mean luminosity and a mean diameter which combines in Eq. (9) to give the value which was independently inferred using available local data: the high redshift galaxies in the $S_{60}$ sample are compatible with the hypothesis of being the progenitors of local galaxies having a standard physical size of $D_{60} = 4.30\ h_{70}^{-1}$ kpc and an absolute luminosity $M_{60} = -18.80 + 5 \log h_{70}$, as derived using the SFI++ sample in Paper II.

The consistency test performed using the $\eta$ indicator assures us that velocities measured using different methods both locally and at high redshift are free of systematics. Galaxies with velocity $v$ at high redshift may actually have intrinsic luminosities and diameters different from those determined for the local sample of galaxies with similar velocity. But there is no evidence against the hypothesis that they are embedded in dark matter halos of similar masses. Moreover, if the halo mass does not change across cosmic time (for example by merging or accretion phenomena), galaxies with velocity $v$ estimated using OII linewidths at high redshift will eventually evolve into local galaxies having linear size and absolute luminosity compatibles with the values predicted by the Tully-Fisher relations ($D(v)$ and $M(v)$) locally calibrated using $H_\alpha$ rotation curves.

### 3.2. Velocity selection of rotators: proof of concept

After checking the consistency of the strategy to select rotators based on the use of different spectral emission lines and different velocity indicators at different redshifts, we now show that, by selecting low/high velocity rotators, we effectively identify distinct classes of small/big disc galaxies which can be used for cosmological studies.

In the right panel of Fig. 2 we plot the intrinsic linear diameter of the high redshift rotators recovered by assuming a flat, lambda-dominated cosmology ($\Omega_{\rm m} = 0.3$, $\Omega_\Lambda = 0.7$, $h_{70} = 1$). The relative scatter at a given velocity is comparable to what is found locally. In particular we observe a tighter relationship for big rotators and a looser one for smaller discs. We are however comparing samples of systematically different richness. As a matter of fact, because of the specific form of the galaxy mass function, the number density of rotators decreases as a function of velocity (e.g. White & Frenk 1991; Marinoni & Hudson 2002). This plot confirms that a tight selection in rotational velocity space translates into a tight selection in diameters, even at high redshift.

In Fig. 2 (left panel), we also show the angular diameter-redshift diagram for our sample of high redshift objects. While no obvious relation seems to exist between the apparent angular dimension and its redshift, by separating the sample into rotational velocity classes ($S_{60}$ and $S_{143}$) evidence for this relation starts to appear; the angle subtended by galaxies in the low-velocity sample are systematically lower, at any redshift, with respect to those of faster rotators. The tightness of the relation becomes even clearer when the theoretically expected $\theta$ vs. $z$ scaling relations are overplotted (the theoretical $\theta(z)$ relation assumes the intrinsic size of the galaxies given in Table 2 and a flat, Λ-dominated cosmology).

## 4. Cosmology-evolution diagram at $z = 1$

As shown in Paper I, if we assume that the evolution of discs is linear with redshift (or can be linearly approximated in the redshift range of interest) and mild (less then 30% at $z = 1.5$),

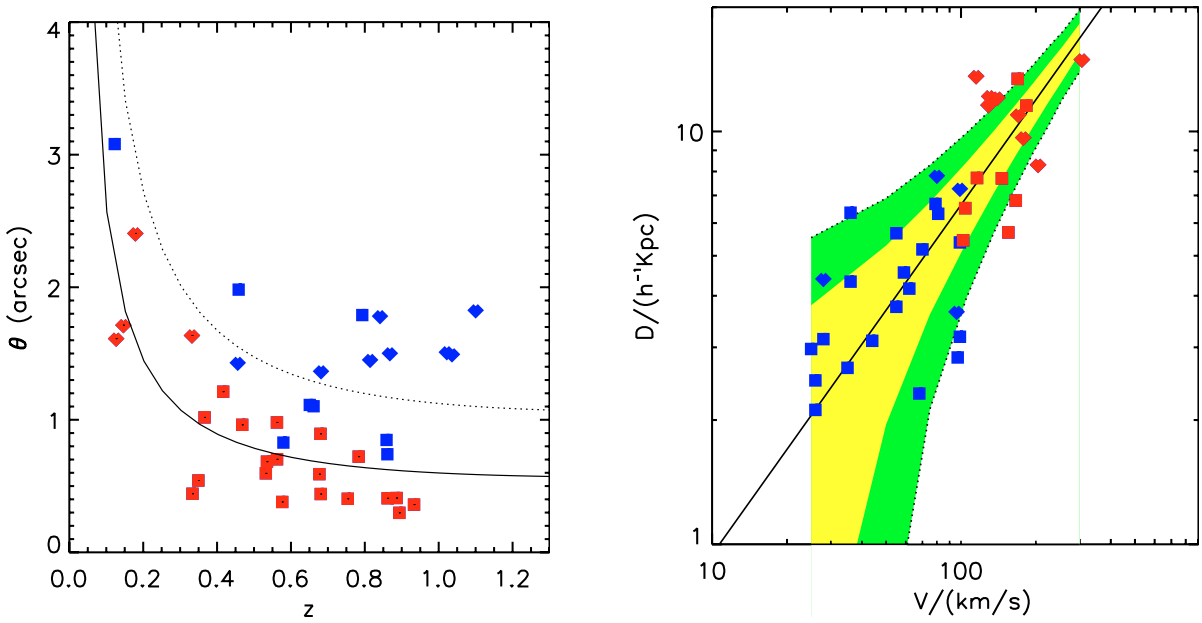


**Fig. 2.** *Left*: angular diameter-redshift diagram for galaxies with $0 < v < 100$ km s$^{-1}$ (red points) and $100 < v < 200$ km s$^{-1}$ (blue points). Galaxies for which HST images are available are indicated with a square. Diamonds represent galaxies with ground photometry (EIS catalog; Arnouts et al. 2001). The angular diameter scaling predicted in a flat, $\Lambda$-dominated cosmology ($\Omega_{\rm m} = 0.3$, $\Omega_\Lambda = 0.7$) is shown. The theoretical expectation has been derived assuming as standard rods the locally ($z = 0$) calibrated half-light diameters of galaxies (see Table 2) at the characteristic velocity corresponding to the mean of the observed velocity distribution of galaxies in the two velocity ranges considered. These values are $D(z = 0, v = 60\ {\rm km\,s^{-1}}) = 4.3\ h_{70}^{-1}$ kpc for the $S_{60}$ sample (solid line) and $D(z = 0, v = 143\ {\rm km\,s^{-1}}) = 9\ h_{70}^{-1}$ kpc for the $S_{143}$ sample (dotted line). *Right*: the inferred half-light diameter $D$ for the $S_{60}$ (red) and $S_{143}$ (blue) samples of galaxies is plotted as a function of the rotational velocity of galaxies. The same cosmology as before is assumed for converting angles into linear diameters. The local calibration for the diameter-velocity relationship (see Eq. (3) of Paper II) is overplotted together with $1\sigma$ and $2\sigma$ uncertainties in the zero-point calibration (shaded area).

then one can use the angular diameter-redshift test to detect in a direct way the eventual presence of a dark energy component. Since our data are still too sparse for placing any meaningful constraint onto this cosmological parameter, we here use our sample to construct the cosmology-evolution plane (see Sect. 6.2 of Paper I).

This diagram allows us to visualize the set of cosmological parameters which are compatible with a given interval of disc/luminosity evolution, and vice versa how much evolution is expected given a specific cosmology. It establishes a one-to-one correspondence between cosmology and the amount of evolution in disc or luminosity at a given redshift.

Given the local calibration for diameters and magnitudes of galaxies within a particular velocity interval, we construct the angular diameter-redshift and Hubble diagrams in any possible cosmological model $\boldsymbol{p}$ spanning the range $p_1 = \Omega_{\rm m} = (0, 1)$ and $p_2 = \Omega_\Lambda = (0, 1)$. We then solve for the set of points $\boldsymbol{p}$ of the parameter space which satisfy the condition

$$\delta_{\rm l}(\bar{z}) < \frac{\epsilon_D(\bar{z}, \boldsymbol{p})}{D(0)} < \delta_{\rm u}(\bar{z}) \qquad (10)$$

where $\delta_{\rm l}$ and $\delta_{\rm u}$ are the lower and upper limits in relative disc evolution at redshift $z = \bar{z}$. For consistency, we thus require that the amount of evolution having to be introduced in order for both sizes ($\epsilon_D(z, \boldsymbol{p}) = D_v(z, \boldsymbol{p}) - D_v(0)$) and luminosities ($\epsilon_{\rm M}(z, \boldsymbol{p}) = M_v(z, \boldsymbol{p}) - M_v(0)$) to fit observations, be compatible with Eq. (6) which describes the *observed* evolution of the intrinsic mean surface brightness within the HLD of the objects, a cosmology-independent observable.

Solving for Eqs. (6) and (10) we can thus construct a self-consistent cosmology-evolution plane, where to any given upper/lower limit for the evolution of diameters or luminosity at $z = \bar{z}$ corresponds in a unique way a specific region of the cosmological parameter space. In Fig. 3 we show the cosmology-evolution diagram for both the $S_{60}$ and $S_{143}$ samples at redshift $z = 1$. This plot establishes a direct link between global properties of the cosmological background, such as curvature, dark matter and dark energy content, and the local structural parameters of rotators.

Let's assume that the luminosity of $v = 200$ km s$^{-1}$ rotators cannot be fainter at $z = 1$, which means that the light output of high redshift rotators hosted in dark matter halos of $v = 200$ km s$^{-1}$ cannot be smaller than that emitted by present day galaxies hosted in such halos. This can be expressed as the following boundary condition for the luminosity evolution of the fast rotators: $\Delta M(z = 1) \leq 0$. Therefore, we assume that the luminosity produced per unit mass is declining (or at most constant) since $z = 1$, and since we are considering halos of similar mass, that galaxies as a whole have been fading away. By inspecting the cosmology-evolution diagram for the $S_{143}$ sample we can conclude, using this a-priori constraint, that a flat, matter-dominated cosmology ($\Omega_{\rm m} = 1$) is excluded at a confidence level of $\sim 3\sigma$. Even more interestingly, the $\Delta M(z) \leq 0$ constraint allows us to conclude that an open cosmology with low mass density ($\Omega_{\rm m} \sim 0.3$) and with no dark energy contribution ($\Omega_\Lambda$) is excluded at a confidence level greater than $1\sigma$.

We stress that these cosmological conclusions are drawn by assuming that, whatever the strength of the luminosity evolution of galaxies with redshift, this evolution cannot lead to the brightening $v = 200$ km s$^{-1}$ rotators from $z = 1$ to the present time. We include evolution in our analysis from the beginning, and we only reject *a-posteriori* cosmological models that are associated at a particular cosmic epoch ($z = 1$ in our case) with unlikely galaxy evolutionary models.

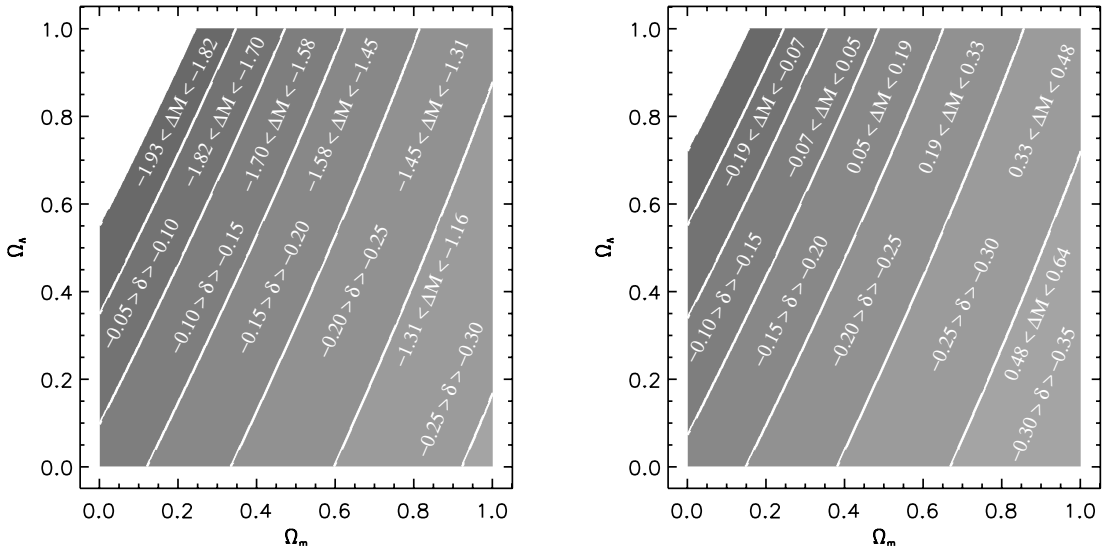


**Fig. 3.** *Left*: cosmology-evolution diagram for the $S_{60}$ sample at $z = 1$. The cosmological plane is partitioned with different boundaries obtained by solving equation 10 for different values of $\delta$, i.e. of the relative evolution in disc size at $z = 1$. Boundaries corresponding to different relative disc evolutions from $\delta = 0$ to $\delta = -30\%$ in steps of 5% intervals are shown. We also show the set of possible absolute luminosity evolutions at $z = 1$ which are compatible with a given set of cosmological models. These upper/lower limits in luminosity evolution have been derived by using Eq. (6). Boundaries in disc relative evolution ($\delta$) are uncertain by a 23% factor, while luminosity evolution boundaries are uncertain by 0.27 mag. *Right*: the same but for the $S_{143}$ sample of higher mass objects. Disc relative evolution boundaries are uncertain by a 20% factor, while luminosity evolution boundaries are uncertain by 0.2 mag.

## 5. Diameter and luminosity evolution in a $\Lambda$*CDM* cosmological model

Insights into the mechanisms of galaxy evolution are traditionally accessible through the study of disc galaxy scaling relations, such as the investigation of the time-dependent change in the magnitude-velocity (Tully-Fisher) relation (e.g., Vogt et al. 1996; Böhm et al. 2004; Bamford et al. 2006), of the magnitude-size relations (e.g., Lilly et al. 1998; Simard et al. 1999; Bouwens & Silk 2002; Barden et al. 2005), or of the disc "thickness" (Reshetnikov et al. 2003; Elmegreen et al. 2005). Yet owing to sample selection effects, and differences in analysis techniques, these studies have come to widely divergent conclusions. In this study, we have explored and adopted a different approach: we infer information about size and luminosity evolution of galaxies by constructing their respective angular diameter-redshift and Hubble diagrams in a fixed reference cosmology.

In Figs. 4 and 5 we show the angular diameter-redshift and Hubble diagrams for the $S_{60}$ and $S_{143}$ samples, respectively. The expected scaling in the flat, $\Lambda$-dominated cosmology with $\Omega_m = 0.3$ and $\Omega_\Lambda = 0.7$ is shown together with the best fitting function obtained by assuming a simple linear redshift evolution for both diameters and absolute magnitudes. Both diameters and angles for the 2 velocity samples are normalized at $z = 0$ by using the values derived in Paper II and shown in Table 2.

The disc and luminosity evolution in a $\Lambda CDM$ cosmology for both small and large rotators is shown in Figs. 6 and 7, respectively. In these figures, we also show how these theoretically-derived evolutionary patterns combine together to give the evolution of the intrinsic surface brightness (see Eq. (5)), and how this last quantity compares to the observed one, which as stated earlier does not depend on the adopted cosmological model.

As stressed in Paper I, the test should be performed with big rotators i.e. using bright candles whose selection is unbiased in a flux-limited spectroscopic survey. Our sample of $v = 200$ km s$^{-1}$ meets this criteria. However, because of the specific form of the galaxy luminosity function, our preliminary sample is dominated by small rotators, whose magnitude distribution could be affected by the Malmquist bias: the observed distribution of galaxies might not include the fainter tail of members having a rotation velocity satisfying our selection criteria ($0 < v < 100$). Even though he GOODs catalog is virtually unbiased in surface brightness selection for the magnitude range considered in this paper, our measurements of surface brightness evolution could be biased simply because of the flux cut at $I = 24$ characterizing our sample. One could in principle miss low surface brightness galaxies of the same size as those observed, simply because their magnitudes are fainter then the survey limit. However, using the low redshift SFI++ sample we have checked that galaxies that are on the faint end tail of the magnitude distribution also tend to be the smaller discs. Therefore, no Malmquist effect is expected to contaminate the observed intrinsic surface brightness evolution.

The spectroscopic survey in the CDFS region is flux-limited at $I < 24$. Since the standard candle of the $S_{60}$ sample has an absolute luminosity $M_{60} = -18.8 + 5 \log h_{70}$ while the brighter luminosity sampled at $z = 1$ is $M = -20.2 + 5 \log h_{70}$, we could be overestimating the observed evolution in luminosity. The fact that we see in our $I = 24$ magnitude-limited sample rotators with $v = 100$ km s$^{-1}$ at $z = 1$ can be interpreted in two different ways: i) these rotators were effectively much brighter in the past, or ii) we only sample the brightest objects, scattered around the standard absolute value. To address the latter, we correct our results for any possible Malmquist bias.

Let's consider the difference between the survey flux limit and the theoretically-predicted best fitting function to the observed magnitude distribution, $\Delta = 24 - m^{\rm bfit}$. A simple estimate of the Malmquist bias is obtained by assuming that the best fitted apparent magnitude is systematically overestimated as a function of distance by the additive quantity $3\sigma - \Delta(z)$, where we assume that the scatter in the standard candle calibration is constant as a function of redshift. In other words, we assume that the galaxies

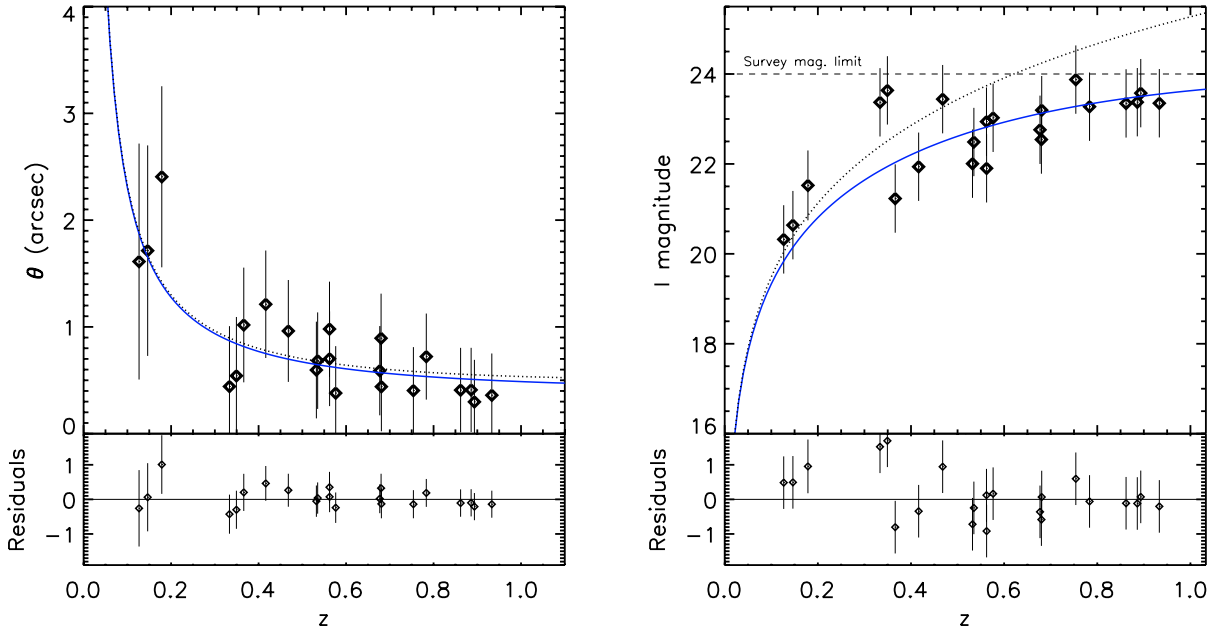


**Fig. 4.** *Left*: angular diameters versus redshift for the $S_{60}$ sample. The dotted line represents the theoretical scaling (Eq. (6)) predicted assuming a standard rod of size $D_{60}(z=0) = 4.3\, h_{70}^{-1}$ kpc and a ΛCDM background cosmological model with parameters $(\Omega_{\rm m} = 0.3, \Omega_\Lambda = 0.7)$. The solid line represent the best fitting linear evolutionary model obtained by assuming $\epsilon_D = \alpha z$ in Eq. (4). Errorbars represent the uncertainties in the calibration of the local standard rod (see Table 2) $\sigma_D/D \sim 0.6$. *Right*: hubble diagram for the $S_{60}$ rotators. The dotted line represent the theoretical scaling predicted assuming a standard candle of absolute luminosity $M_{60}(z=0) = -18.80 + 5\log h_{70}$ and the same cosmology as before. The solid line represents the best fitting linear evolutionary model for luminosities obtained by using $\epsilon_M = \beta z$ in Eq. (1). Errorbars represent the uncertainties in the calibration of the local standard candle (see Table 2) $\sigma_{\rm m} = 0.75$.

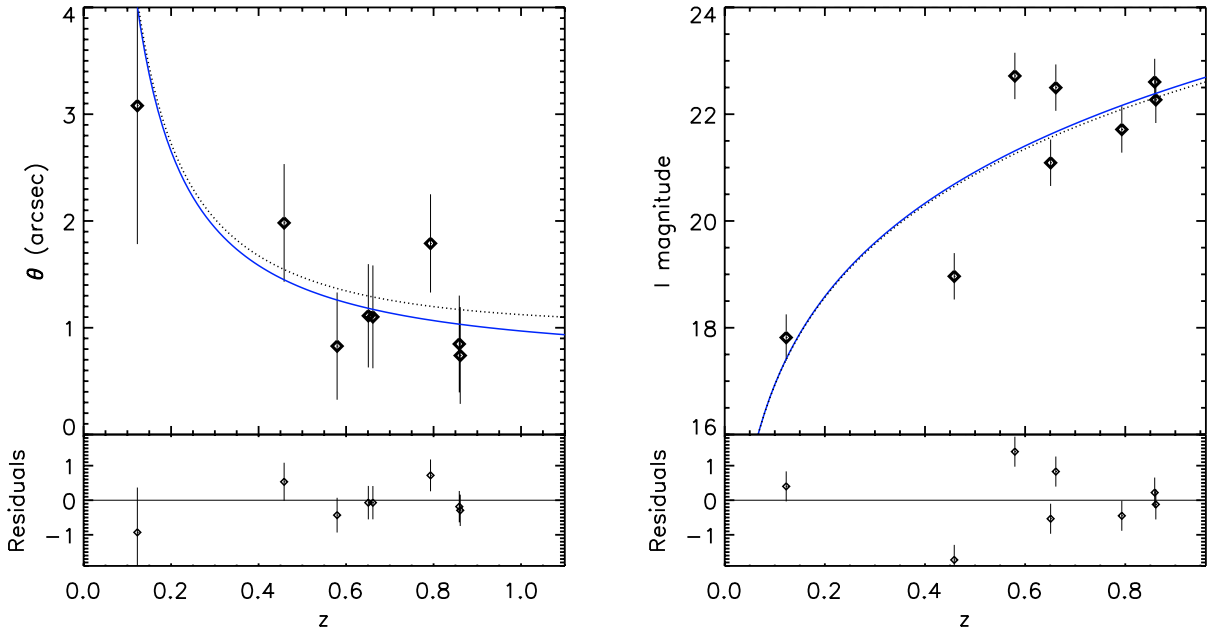


**Fig. 5.** The same as in Fig. 4 but for the $S_{143}$ sample of rotators. Errorbars in the angular diameter-redshift diagram (*left*) represent the uncertainties in the calibration of the local standard rod (see Table 2) $\sigma_D/D \sim 0.3$. Errorbars in the Hubble-diagram (*right*) represent the uncertainties in the calibration of the local standard candle (see Table 2) $\sigma_{\rm m} = 0.2$.

we see are the brighter subset of standard rods whose luminosity scatters around $M_{60}$.

We have implemented this correction consistently both for galaxy luminosities and diameters. The incidence of the Malmquist bias on our conclusions is graphically shown in Fig. 6. Due to the strong influence of the Malmquist correction term, the observed disc and luminosity evolution for the slow rotators sample $S_{60}$ is compatible with the following diametrically opposite interpretations: i) data are affected by the Malmquist bias and therefore small discs have undergone almost no luminosity evolution but a strong size evolution (they were nearly 50% smaller at $z = 1$ than at present epoch), or ii) data are unaffected by the Malmquist bias and the small discs have undergone strong luminosity evolution but not much size evolution since $z \sim 1$.

Since there is marginal evidence that the scatter around the expected disc and luminosity evolution is decreasing as redshift increases (see Fig. 6), we take a conservative position and

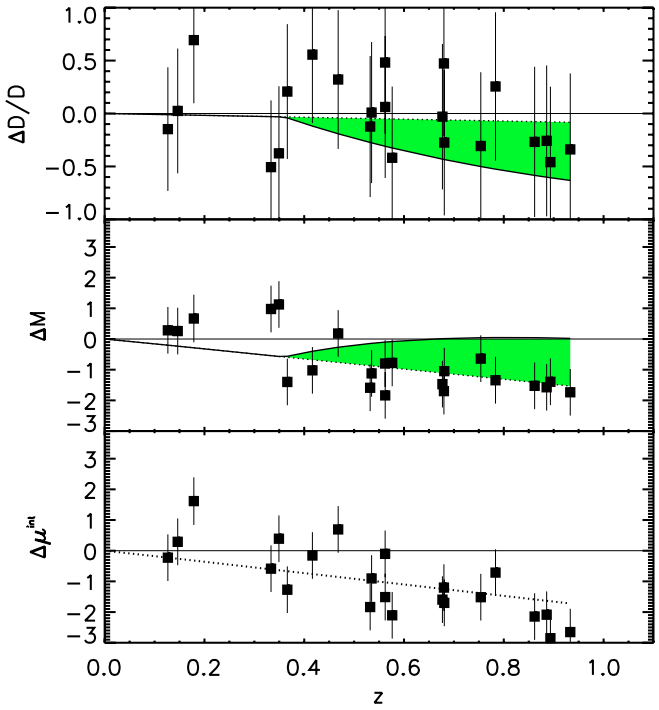


**Fig. 6.** *Top*: relative evolution in the diameter size for the $S_{60}$ sample of low velocity rotators. We assume the zeropoint diameter normalization quoted in Table 2 and a a ΛCDM cosmological framework. Errorbars represent $1\sigma$ scatter in the calibration of the local standard rod. The dotted line represent the best fitting linear evolutionary model for diameters obtained by assuming $\epsilon_D = \alpha z$ in Eq. (4). The solid line represents the upper limit on relative disc evolution estimated by correcting for the Malmquist bias affecting the data. *Center*: evolution of the absolute magnitude of galaxies in the $S_{60}$ sample and in a ΛCDM cosmological framework. We assume as standard luminosity the mean absolute magnitude of a sample of similar rotators at $z \sim 0$ (see Table 2). Errorbars represent $1\sigma$ scatter in the calibration of the local standard candle. The dotted line represent the best fitting linear evolutionary model for luminosities obtained by using $\epsilon_M = \beta z$ in Eq. (1). The solid line represents the inferior limit on absolute magnitude evolution estimated by correcting for the Malmquist bias affecting the data. *Bottom*: evolution in the intrinsic surface brightness within the half-light diameter. This evolution is independent of the particular cosmological background. The dotted line represents the combination (Eq. (6)) of the best fitting diameter and luminosity evolution functions.

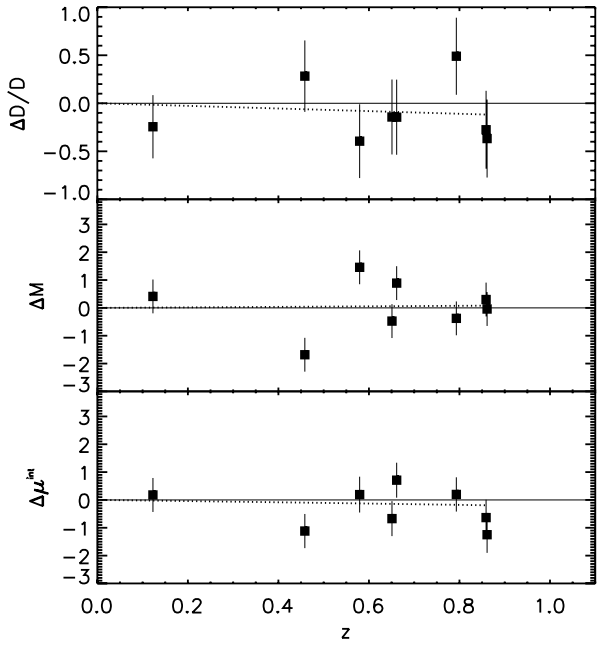


**Fig. 7.** Same as Fig. 6 but for the $S_{143}$ sample.

assume, in the following, that our $S_{60}$ sample is affected by the Malmquist bias. Only a sample of small rotators selected in a magnitude-limited survey deeper than the CDFS will allow to unambiguously resolve the issue by differentiating between the two opposite scenarios. However, we stress again that the large rotators sample $S_{143}$ does not suffer from Malmquist bias selection effects.

## 6. Discussion on the evolution of structural parameters

Assuming a $\Lambda CDM$ cosmology, several conclusions can be reached about the evolution of the structural parameters of fixed-velocity rotators.

1. The surface brightness evolution of discs is significantly different for the two populations, $S_{60}$ and $S_{143}$: $\Delta\mu = -1.90 \pm 0.35$ mag/arcsec$^2$ for the slow rotators ($S_{60}$) and $\Delta\mu = -0.25 \pm 0.27$ mag/arcsec$^2$ for the fast rotators ($S_{143}$).
2. The fast rotators show neither significant size nor luminosity evolution since $z = 1$.
3. Under the conservative assumption that most of the luminosity difference over redshift for the small rotators is due to the Malmquist bias, they appear to have gone through a significant size evolution and no luminosity evolution since $z = 1$. (however the opposite is true in the limiting case in which Malmquist bias minimally affects our low-velocity data. In this case, small discs have undergone strong luminosity evolution but not much size evolution since $z \sim 1$.)

The results presented in the previous section highlight the potential of the geometrical tests, not only to constrain cosmological parameters, but also to derive information about the evolution of galaxy structural parameters. However, the extent of the analysis that can be performed at this point is significantly reduced by the small sample of galaxies available with deep photometry and high resolution spectroscopic measurements, and by the limiting magnitude of the CDFS. This magnitude limit introduces a potentially very strong Malmquist bias for the sample of small discs, $S_{60}$, which prevents us from determining if the surface brightness increase of ∼1.9 mag/arcsec$^2$ of these galaxies at $z = 1$ is due to a strong luminosity or size evolution (or a combination of both). This distinction has not been made by most previous studies either, but could be achieved in the future using the strategy proposed here and a deeper, more complete galaxy sample.

Because at the limiting magnitude of $I = 24$ of the VIMOS spectroscopic survey the GOODs photometric catalog is unbiased in surface brightness selection, conclusions can however be reached about the surface brightness evolution of discs. While we find strong evolution for the small rotators, the large rotators seem to have retained a constant surface brightness since $z = 1$. The evolution of more than one mag/arcsec$^2$ at $z = 1$ for the small discs is consistent with results of previous studies of the magnitude-size relation (e.g. Schade et al. 1996; Forbes et al. 1996; Lilly et al. 1998; Roche et al. 1998; Saintonge et al. 2005; Barden et al. 2005), or of the magnitude-velocity (Tully-Fisher) relation (e.g. Milvang-Jensen et al. 2003; Böhm et al. 2004;

Bamford et al. 2006). While others report very little or no surface brightness evolution (e.g. Simard et al. 1999; Ravindranath et al. 2004), Barden et al. (2005) reconciles this discrepancy by considering the different data analysis techniques. It also seems likely that some of these results are affected by the selection criteria applied. For example, some authors selected their samples on the basis of blue colors (Rix et al. 1997), strong emission line equivalent widths (Simard & Pritchet 1998), or large disc sizes (Vogt et al. 1996). The two former criteria prefer late-type spirals, whereas the latter criterion leads to the overrepresentation of large, early-type spirals. With our strategy, based on a spectroscopic follow-up of objects with OII emission-lines selected from a purely flux-limited redshift survey, biases are largely reduced.

In Sect. 3.1, we have shown that the two classes of galaxies at high redshift with rotation velocity estimated on the basis of their OII linewidths represent in an unbiased way the progenitors of local discs whose velocity is inferred using the H$\alpha$ rotation curves. We stress that this statement does not imply that every high redshift galaxy with the same rotational velocity as a local galaxy is its direct progenitor. Due to the prevalence of mergers, interactions and accretion phenomena in the past, this is actually an unlikely scenario. What the $\eta$-test guarantees is that the high- and low-$z$ samples represent the same populations of rotators with nearly the same mass. While interactions were more frequent in the past, are known to lead to the onset of star formation events and could therefore provide an explanation of the excess in luminosity of the small discs at high $z$, all the ACS images were examined and show that all the galaxies in the sample are not undergoing merger events.

Under the hierarchical scenario for the growth of structure, the following scaling relation for the disc scalelength, $R_{\rm d}$, of dark matter systems is predicted (Mo et al. 1998):

$$R_{\rm d} \approx 8.8\, h^{-1}{\rm kpc}\left(\frac{\lambda}{0.05}\right)\left(\frac{V_{\rm c}}{250\ {\rm kms}^{-1}}\right)\left(\frac{H(z)}{H_0}\right)^{-1}\left(\frac{j_{\rm d}}{m_{\rm d}}\right)$$

where $\lambda$ is the disc spin parameter, $V_{\rm c}$ the circular velocity, $j_{\rm d}$ the angular momentum of the disc as a fraction of that of the halo, and $m_{\rm d}$ is the disc mass as a fraction of that of the halo. Since there is no dependency of $\lambda$ on redshift and since $j_{\rm d}/m_{\rm d} = 1$ if discs are formed while conserving specific angular momentum, the disc scalelength of dark matter systems having a given circular velocity scales as

$$R_{\rm d} \propto H^{-1}(z), \tag{11}$$

where $z$ corresponds to the redshift of formation of the galactic discs. Under the fairly safe assumption that the diameter of the stellar disc of a galaxy scales with the scalelength of its dark matter halo, the diameter of our velocity-selected standard rods should also evolve as $D \propto H^{-1}(z)$. This relation therefore predicts that discs forming at the present epoch should be larger by a factor of 1.8 than those that formed at $z = 1$. This estimate agrees with our most pessimistic scenario for the Malmquist bias, which asks for the small discs to be larger by a factor of two at $z = 0$.

Interestingly, the fact that no size evolution is seen for the large rotators may tell us something about the time of formation of these systems. In Eq. (11), the dependency of the radius $R_{\rm d}$ is on the value of the Hubble constant *at the epoch of last assembly of the discs*. This corresponds to the last time when there was a significant reshuffling of the disc (i.e. the last incidence of a major merger). Since the discs in our $S_{60}$ sample show size evolution that is consistent with Eq. (11), the redshifts at which we observe them probably coincide with the epochs at which these systems are still forming. Due to the paucity of the galaxy sample at hand, no firm conclusion can be reached at this point, but there are some hints that the large discs were already in place by $z = 1$ while most of the small discs have assembled since then. There is tantalizing evidence of a similar effect in the scaling relation between disc scalelength and rotation velocity observed for nearby galaxies, where the smallest discs appear to be consistent with an epoch of last formation at $z < 0.5$ while this is pushed back at $0.5 < z < 1.0$ for the larger systems (Spekkens 2005).

Note that a relation similar to Eq. (11) also exists for the disc surface density, $\Sigma_0$. However, it is not as straightforward to extend that relation to predict the behavior of surface brightness, because of its dependency on the stellar mass-to-light ratio. Therefore, a similar interpretation can not be made for the observed surface brightness evolution of the discs, as it is not possible to disentangle the combined effects of redshift and mass-to-light ratio evolution.

Finally we note that fast rotators cannot have stopped forming stars at least over the epochs explored in this study. The constancy of their luminosity up to $z = 1$ can be explained in terms of star-formation activity continuously on-going for a Hubble time.

## 7. Conclusions

The goal of this pilot observational program is to investigate the relationship between global properties of the universe (geometric curvature, dark matter and dark energy content) and local structural parameters of disc galaxies (disc linear size and absolute luminosity). To this purpose we apply the angular size-redshift test and the Hubble diagram at the same time to the same class of standard objects, namely, velocity-selected disc galaxies. As such, it presents one of the first attempts to investigate if specific subsamples of high redshift galaxies can be used as cosmological tracers complementary to SNIa and CMB observations. This approach allows us to construct a cosmology-evolution diagram at redshift $z = 1$, the chart that allows for the mapping of the cosmological parameter space onto the disc galaxy structural parameter space (diameter, luminosity and surface brightness). Assuming prior knowledge about disc evolution, this diagram allows us to draw some interesting cosmological conclusions. If we assume that the absolute magnitude evolution is constrained to be negative at $z = 1$ (i.e. it is impossible that $v = 200$ km s$^{-1}$ rotators were fainter at $z = 1$ than at the present time, which means that their luminosity per unit mass was higher in the past), we find with the data at hand that:

1. a flat matter-dominated cosmology ($\Omega_{\rm m} = 1$) is excluded at a confidence level of $2\sigma$;
2. an open cosmology with low mass density ($\Omega_{\rm m} \sim 0.3$) and no dark energy contribution ($\Omega_\Lambda$) is excluded by present data at a confidence level of $1\sigma$.

On the other hand, by fixing the background cosmological model, the cosmology-evolution diagram allows us to investigate the evolution in the structural parameters of disc galaxies which are hosted in dark matter halos of *similar mass*. Assuming a $\Lambda CDM$ model, we find that:

1. while small mass galaxies go through a strong surface brightness evolution of $-1.90\pm0.35$ mag/arcsec$^2$ since $z = 1$, larger discs only evolve by $-0.25 \pm 0.27$ mag/arcsec$^2$;

2. under the assumption that our sample of small discs is affected by the Malmquist bias, this surface brightness evolution is caused by an increase in the size of the fixed-velocity rods by a factor of two from $z = 1$ to the present epoch;
3. discs hosted in more massive halos, which are not affected by the Malmquist bias, show neither size nor luminosity evolution, suggesting that they finished assembling before $z = 1$, unlike the smaller discs that are still undergoing formation at $z < 0.5$.

We conclude that the luminosity evolution observed is coherent with the emerging picture of a differential star formation history for galaxies of different masses (Juneau et al. 2005). These results are also consistent with the growth of structure predicted in the universe described by the concordance cosmological model (Mo et al. 1998; Bower et al. 2006).

In this preliminary study we are still limited by the small number statistics affecting our sparse sample. While with a larger sample of high resolution spectra and images one can detect in a direct way the eventual presence of a dark energy component (see Paper I), it was not possible to apply the angular diameter-redshift test and put a constraint on its amplitude and on its equation of state parameter $w$ with the amount of data currently available. For the same reason, galaxies were separated in only two velocity bins to construct the cosmology-evolution diagram. This limits the class of mass-selected objects for which we can trace evolution across different cosmic epochs. The availability of a larger sample will allow finer velocity bins, and therefore less scatter in the results.

To conclude, we reiterate that the rotational velocity of distant galaxies, when interpreted as a size (luminosity) indicator, may be used as an interesting tool to select high redshift standard rods (candles). Though the power of geometrical tests to constrain fundamental cosmological parameters has long been recognized, only with the recent large, deep redshift surveys have their implementation been made possible. With only a limited amount of data but a novel and physically justified technique to select standard rods/candles, we have shown that these tests can give useful insights not only on the value of fundamental cosmological parameters, but also the time evolution of fundamental galaxy observables in mass-selected disc rotators.

*Acknowledgements.* We wish to thank the referee for many useful comments and suggestions. This work has been partially supported by NSF grants AST-0307661 and AST-0307396 and was done while A.S. was receiving a fellowship from the *Fonds de recherche sur la Nature et les Technologies du Québec*. C.J.W. is supported by the MAGPOP Marie Curie EU Research and Training Network. K.L.M is supported by the NSF grant AST-0406906. The VLT-VIMOS observations have been carried out on guaranteed time (GTO) allocated by the European Southern Observatory (ESO) to the VIRMOS consortium, under a contractual agreement between the Centre National de la Recherche Scientifique of France, heading a consortium of French and Italian institutes, and ESO, to design, manufacture and test the VIMOS instrument.

## References

Arnouts, S., Benoist, C., Vandame, B., et al. 2001, A&A, 379, 740
Bamford, S. P., Aragón-Salamanca, A., & Milvang-Jensen, B. 2006, MNRAS, 366, 308
Barden, M., Somerville, R. S., Rix, H.-W., et al. 2005, ApJ, 635, 959
Böhm, A., Saglia, R. P., Ziegler, B. L., et al. 2004, A&A, 420, 97
Bottini, D., Garilli, B., Maccagni, D., et al. 2005, PASP, 117, 996
Bouwens, R., & Silk, J. 2002, ApJ, 568, 522
Bower, R. G., Benson, A. J., Malbon, R., et al. 2006, MNRAS, 370, 645
de Jong, R. S. 1996, A&A, 313, 377
Elmegreen, D. M., Elmegreen, B. G., Rubin, D. S., & Schaffer, M. A. 2005, ApJ, 631, 85
Ferguson, H. C., Giavalisco, M., Dickinson, M., et al. 2004, ApJ, 600, L107
Forbes, D.A., Phillips, A. C., Koo, D. C., & Illingworth, G. D., 1996, ApJ, 462, 89
Giavalisco, M., Ferguson, H. C., Koekemoer, A. M., et al. 2004, ApJ, 600, L93
Ilbert, O., Tresse, L., Zucca, E., et al. 2005, A&A, 439, 863
Juneau, S., Glazebrook, K., Crampton, D., et al. 2005, ApJ, 619, L135
Le Fèvre O., Paltani, S., Vettolani, G., et al. 2004, A&A, 428, 1043
Le Fèvre O., Garilli, B., Vettolani, G., et al. 2005, A&A, 439, 845
Lilly, S. J., Ellis, R., Schade, D., et al. 1998, ApJ, 500, 75
Lilly, S. J., Le Fevre, O., Renzini, A., et al. 2006, ApJS, 172, 70
Lima, J. A. S., & Alcaniz, J. S. 2001, A&A, 566, 15
Madau, P., Ferguson, H. C., Dickinson, M. E., et al. 1996, MNRAS, 283, 1388
Marinoni, C., & Hudson M., 2002, ApJ, 569, 101
Marinoni, C., & Le Fèvre, O. 2004, Ap&SS, 290, 195
Marinoni, C., Saintonge, A., Giovanelli, R., et al. 2008, A&A, 478, 43
Milvang-Jensen, B., Aragón-Salamanca, A., Hau, George K. T., & Jørgensen, I. 2003, MNRAS, 339, L1
Mo, H. J., Mao, S., & White, S. D. M. 1998, MNRAS, 295, 319
Oke, J. B., & Gunn, J. E. 1983, ApJ, 266, 713
Ravindranath, S., Ferguson, H. C., Conselice, C., et al. 2004, ApJ, 604, L9
Reshetnikov, V. P., Dettmar, R.-J., & Combes, F. 2003, A&A, 399, 879
Rix, H.-W., Guhathakurta, P., Colless, M., & Ing, K. 1997, MNRAS, 285, 779
Roche, N., Ratnatunga, K., Griffiths, R. E., Im, M., & Naim, A. 1998, MNRAS, 293, 157
Saintonge, A., Schade, D., Ellingson, E., Yee, H. K. C., & Carlberg, R. G. 2005, ApJS, 157, 228
Saintonge, A., Masters, K.L., Marinoni, C., et al. 2008, A&A, 478, 57
Sandage, A. 1988, ARA&A, 26, 561
Sandage, A., & Perelmuter, J.-M. 1990, ApJ, 350, 481
Sandage, A., Kron, R.G., Longair, M. S., Binggeli, B., & Buser, R. 1995, The Deep Universe, Saas-Fee Advanced Course 23. Lecture Notes 1993, Swiss Society for Astrophysics and Astronomy, ed. B. Bingelli & R. Buser (Berlin: Springer-Verlag)
Schade, D., Carlberg, R. G., Yee, H. K. C., Lopez-Cruz, O., & Ellingson, E. 1996, ApJ, 465, L103
Schlegel, D. J., Finkbeiner, D. P., & Davis, M. 1998, ApJ, 500, 525
Simard, L., & Pritchet, C. J. 1998, ApJ, 505, 96
Simard, L., Koo, D. C., Faber, S. M., et al. 1999, ApJ, 519, 563
Spekkens, K. 2005, Ph.D. Thesis, Cornell University
Springob, C. M., Masters, K. L., Haynes, M. P., Giovanelli, R., & Marinoni, C. 2007, ApJS, in press [arXiv:astro-ph/07050647]
Stoughton, C., Bernardi, M., Lupton, R. H., et al. 2002, AJ, 123, 485
Tresse L., et al. 2006, A&A 472, 403
Tully, R. B., & Fisher, J. R. 1977, A&A, 54, 661
Tully, R. B., Pierce, M. J., Huang, J.-S., et al. 1998, AJ, 115, 2264
Vogt, N. P., Forbes, D. A., Phillips, A. C., et al. 1996, ApJ, 465, L15
White, S. D. M., & Frenk, C. S., 1991, ApJ, 379, 52